Original article

Use of a novel Screen–Enrich–Combine(-biomaterials) Circulating System to fill a 3D-printed open Ti6Al4V frame with mesenchymal stem cells/β-tricalcium phosphate to repair complex anatomical bone defects in load-bearing areas

Wenxiang Chu[1,2#], Zhiqing Liu[1#], Yaokai Gan[1], Yongyun Chang[1], Xin Jiao[1], Wenbo Jiang[1], Kerong Dai[1]

[1]Shanghai Key Laboratory of Orthopedic Implants, Department of Orthopedic Surgery, Shanghai Ninth People's Hospital, Shanghai Jiao Tong University School of Medicine, Shanghai, China; [2]Department of Orthopedic Surgery, Changzheng Hospital, Naval Medical University, Shanghai, China

Contributions: (I) Conception and design: Y Gan, W Chu; (II) Administrative support: K Dai; (III) Provision of study materials or patients: W Jiang; (IV) Collection and assembly of data: W Chu, Z Liu, X Jiao; (V) Data analysis and interpretation: W Chu, Y Chang; (VI) Manuscript writing: All authors; (VII) Final approval of manuscript: All authors.

[#]These authors contributed equally to this work.

Correspondence to: Yaokai Gan. Shanghai Key Laboratory of Orthopedic Implants, Department of Orthopedic Surgery, Shanghai Ninth People's Hospital, Shanghai Jiao Tong University School of Medicine, Shanghai 200011, China. Email: ganyk2004@126.com.

Background: Repairing complex anatomical load-bearing bone defects is difficult because it requires the restoration of the load-bearing function, reconstructing the anatomical shape, and repair by regenerated bone. We previously developed a Screen–Enrich–Combine(-biomaterials) Circulating System (SECCS) for rapid intraoperative enrichment of autologous bone marrow mesenchymal stem cells (MSCs) to enhance the osteogenic ability of porous bone substitutes. In this study, we prepared a 3D-printed Ti6A14V macroporous frame matching the defect shape to provide early load-bearing support and evaluated the efficacy of filling the frame with SECCS-processed MSCs/beta tricalcium phosphate (β-TCP) for long-term bone growth.

Methods: Fifteen 2-year-old goats were involved in this study, and the lateral part of their distal femur was removed by an electric saw and was fitted by a matching electron beam melting technology-prepared (EBM) Ti6Al4V frame. Three types of frames, filled with nothing, pure porous β-TCP, or SECCS-processed MSCs/β-TCP, were fixed onto the defect site. Repair efficacy was evaluated by X-ray radiography, computed tomography (CT), histology, and histomorphometry.

Results: In the basic regular hexagon printing unit, the combined side width (w) and the inscribed circle diameter (d) determines the printing frame's mechanical strength. The compressive load was significantly higher for w=1.9 mm, d=4.4 mm than for w=1.7 mm, d=4.0 mm or w=2.0 mm, d=5.0 mm ($P<0.05$). The EBM-prepared Ti6Al4V defect-matched frame was well maintained 9 months after implantation. The MSCs successfully adhered to the wall of the porous β-TCP in the SECCS-processed group and had spread fully in the test samples. Each goat in the MSCs/β-TCP–the filled group, had approximately 31,321.7±22,554.7 of MSCs and a larger area of new bone growth inside the frame than the control and blank areas groups.

Conclusions: Filling the 3D-printed Ti6Al4V large-aperture frame with osteogenic materials achieved biological reconstruction over a larger area of regenerated bone to repair complex anatomical weight-bearing bone defects under the condition of early frame-supported load bearing. MSCs/β-TCP prepared by SECCS can be used as a filling material for this type of bone defect to obtain more efficacious bone repair.

Keywords: 3D printing; enrichment technique; mesenchymal stem cell (MSC); biomaterial; bone repair

Submitted Sep 29, 2020. Accepted for publication Dec 18, 2020.

doi: 10.21037/atm-20-6689

View this article at: http://dx.doi.org/10.21037/atm-20-6689

© Annals of Translational Medicine. All rights reserved.

Introduction

Complex defects in weight-bearing parts of bone are often observed in clinical settings that perform pelvic reconstructions, repairs of bone defects in the acetabulum, femoral condyle, and proximal tibia caused by tumors and operations in patients with severe trauma, infection, and prosthesis-related osteolysis (1-3). Repairs of such complex bone defects are difficult because they require restoration of the load-bearing function, reconstructing the anatomical shape, and repair by regenerated bone, which creates significant clinical challenges. Current treatments focus on one or two of these three tasks since it can be difficult to repair all three at once. For example, structural bone grafts as part of the bone repair cannot tolerate early weight-bearing, and complex morphological reconstruction and metal products, such as pads, cups, and cages that are used to provide weight-bearing during postoperative recovery only allow a very limited volume of autologous bone growth (4-6). Consequently, providing early weight-bearing function in bone reconstruction allows the maximum volume of new bone growth inside a complex anatomically shaped support frame would be the major goal of such defect repair.

The increasing capabilities of 3D printing have enabled the more accurate and personalized reconstruction of complex anatomical structures. Although a 3D-printed microporous structure can permit a certain degree of bone ingrowth, the volume of in-grown bone is still very limited. To achieve maximal reconstruction by new bone, a 3D-printed large-aperture metal frame providing basic mechanical support filled with osteogenic materials inside the frame to achieve long-term regenerated bone filling is currently a more feasible solution. At present, the insufficient amount of autologous bone and limited osteogenic ability of conventional bone substitutes has led to research efforts aimed at identifying bone fillings with excellent osteogenic properties (7-9). The stem cell Screen–Enrich–Combine(-biomaterials) Circulating System (SECCS), developed previously by us, can rapidly prepare enriched mesenchymal stem cell (MSCs)/beta tricalcium phosphate (β-TCP) composites, which have shown good bone repair ability in animal and various clinical bone defect models (10,11). However, the efficacy of repair needs to be further verified as an in-frame filling to repair complex anatomical bone defects.

In this study, we used the lateral half of a goat distal femur as a defect model to assess the ability of 3D-printed large-aperture titanium alloy frames filled with MSCs/β-TCP prepared by SECCS to repair complex anatomical weight-bearing bone defects to provide a new mode of treatment for such bone defects. We present the following article in accordance with the ARRIVE reporting checklist (available at http://dx.doi.org/10.21037/atm-20-6689).

Methods

General experimental design

All experimental procedures in this study were approved and performed under a project license (HKDL [2017] 405) granted by the Animal Ethics Committee of Shanghai Ninth People's Hospital, in compliance with the Shanghai Ninth People's Hospital affiliated with the Shanghai Jiao Tong University School of Medicine guidelines for the care and use of animals. Fifteen 2-year-old Shanghai White goats (40–45 kg) were included and randomly assigned in this study to an experimental group (n=5) that underwent repair with a macroporous titanium alloy (Ti6Al4V) frame filled with SECCS-processed MSCs/β-TCP, a control group (n=5) that underwent repair with a Ti6Al4V frame filled with pure β-TCP, and a blank group (n=5) that underwent repair with an unfilled Ti6Al4V frame. The general experimental protocol is shown in *Figure 1*.

Parameter optimization and mechanical strength verification for the 3D-printed Ti6Al4V frame

A cylindrical testing frame (2.5 cm diameter × 5 cm height) with a basic regular hexagon unit was designed by using Mimics software (Materialise, Belgium). The width of this hexagon's sides (w) and the diameter of the circle inscribed in it (d) were used as the adjustable parameters. Three different combinations of this width and diameter, namely (w=1.7 mm, d=4.0 mm), (w=1.9 mm, d=4.4 mm), and (w=2.0 mm, d=5.0 mm), were used to fabricate the cylindrical Ti6Al4V testing frames by using electron beam melting (EBM) (*Figure 2A*). A mechanical testing machine (Instron 8874; Instron, USA) was used to perform compression tests to compare the three frames' mechanical properties (*Figure 2B,C*). Briefly, the compression tool was connected to the machine, and the load was applied to the testing frame until the frame collapsed. The parameter combination with the best mechanical performance was used to prepare the animal model's frames.

© Annals of Translational Medicine. All rights reserved.

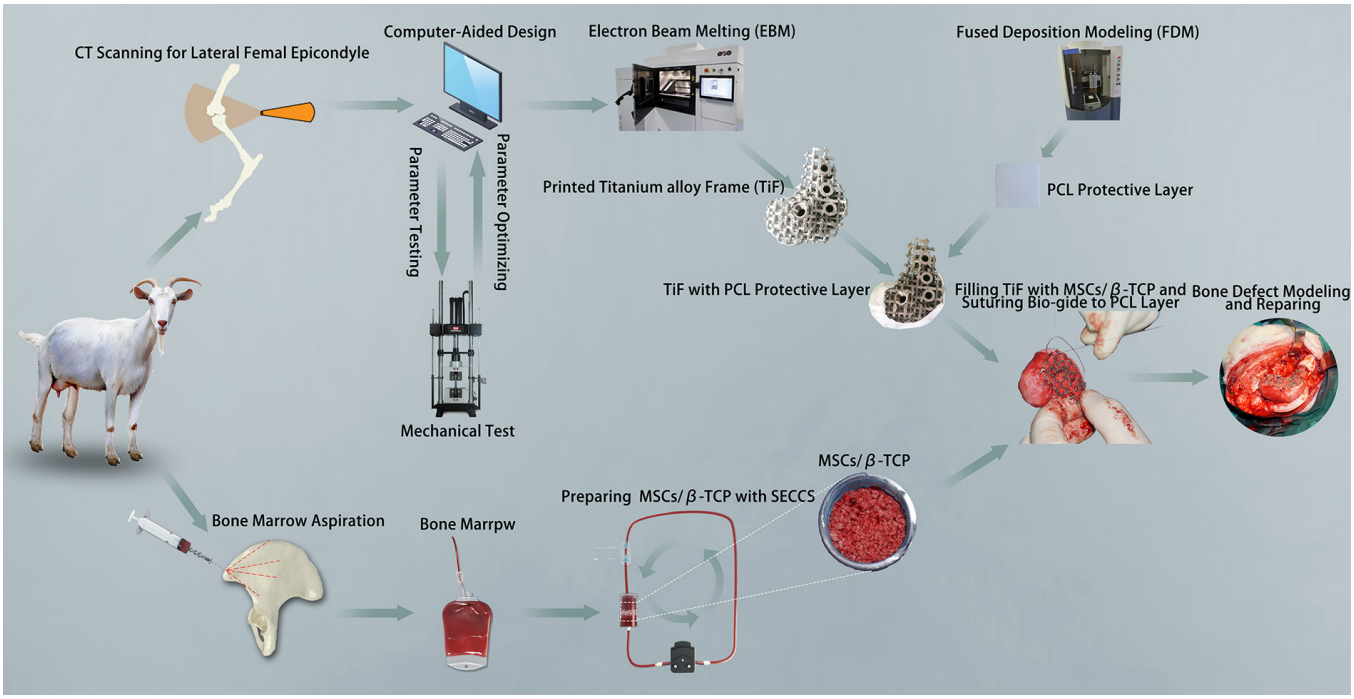

Figure 1 Experimental protocol for the repair of bone defects in the goats' lateral half of the distal femur.

Fabrication of the Ti6Al4V frame and rounding off its distal surface

Computed tomography (CT) data of the goats' right-hind knees were input into the Mimics software to construct frames matched to the lateral half of the distal femurs in the study goats. The basic regular hexagon unit had a side width of 1.9 mm and an inscribed circle diameter of 4.4 mm (*Figure 3A,B,C*). At the same time, the fixing plate and screw position on the frame was also designed. The designed frame and fixing system were fabricated with Ti6Al4V by EBM (*Figure 3D,E,F*). To round the frame's distal surface, a poly (ε-caprolactone) (PCL) membrane with a thickness of 2 mm and a line spacing of approximately 100 μm was prepared by fused deposition modeling. Then, the prepared PCL membrane was softened in a 58 ℃ water bath and attached to the distal surface of the Ti6Al4V frame (*Figure 3G,H,I*).

Preparation and characterization of the MSCs/β-TCP composite

The mixture of MSCs/β-TCP was prepared by SECCS, as previously reported (10). Briefly, after the goat was fully anesthetized, approximately 55 mL of bone marrow was taken from the bilateral anterior superior iliac spines. Two mL of bone marrow was taken for nucleated cells and colony-forming units that express alkaline phosphatase (CFU/ALP+) counting. The remaining bone marrow and 6 g of porous β-TCP (1–3 mm diameter, 75% porosity) were placed in the SECCS for preparation of the MSCs/β-TCP composites. After this process, the bone marrow was reserved for the same counting.

To confirm whether MSCs had successfully combined with β-TCP through SECCS, SECCS-processed MSCs/β-TCP particle testing samples were cultured in Minimum Essential Medium (α-MEM) supplemented with 10% fetal bovine serum at 37 ℃ in 5% CO_2 for 2 weeks. The particles in the samples were then observed by scanning electron microscopy (SEM) and a confocal laser scanning microscope. Before the observation by SEM, the particles were subjected to glutaraldehyde fixation, critical point drying, and then metal spraying. For detection by the confocal laser scanning microscope, the samples were fixed with 4% paraformaldehyde and incubated with 5% Triton-100 for 5 minutes, followed by incubation with rhodamine at room temperature in the dark for 40 minutes and then with 4',6-diamidino-2-phenylindole for 5 minutes.

© Annals of Translational Medicine. All rights reserved.

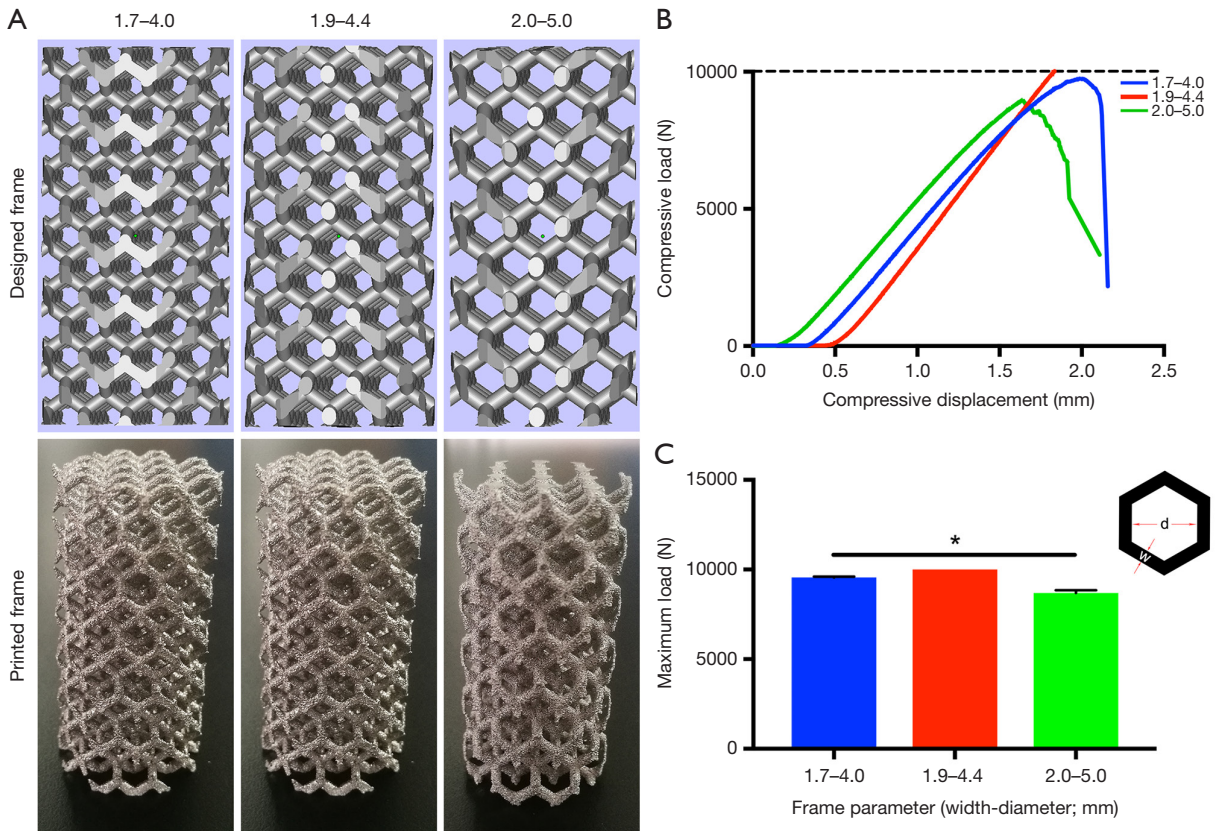

Figure 2 Parameter optimization by mechanical testing for 3D-printing of the Ti6Al4V open frame. (A) Cylindrical frames with hexagonal unit parameters of different side widths and inscribed circle diameters were designed and fabricated with Ti6Al4V. (B) The frame with a 1.9 mm width and a 4.4 mm diameter withstood the machine's extreme load of 10,000 N, and the frames with a 1.7 mm width, 4.0 mm diameter, and a 2.0 mm width, 5.0 mm diameter collapsed before the extreme loading. (C) Comparison of maximum loads between frames with different parameters. (Note: the maximum load of the frame with a 1.9 mm width and a 4.4 mm diameter exceeded the machine's upper limit and was regarded as having the machine's maximum load of 10,000 N).

Establishment and repair of the bone defect model

All animals fasted for 24 hours before anesthesia. General anesthesia was induced via intravenous injection of xylazine (0.15 mL/kg) and 3% pentobarbital sodium (10 mL) and maintained with 3% pentobarbital sodium (3–5 mL) according to the goat's condition. Then, endotracheal intubation and electrocardiographic monitoring were performed. After bone marrow aspiration, each goat's knee was fully exposed, and the lateral half of the distal femur was removed using an electric saw to establish the bone defect model. At the same time, the MSCs/β-TCP particles prepared by SECCS were filled into the Ti6Al4V frame, with a Bio-Gide membrane sutured into the surface of the PCL membrane to protect the joint further. Then, the processed frame was fixed at the defect site by using a customized plate and screws. After the surgery, all animals were administered intramuscular cephazolin (10 mg/kg) once a day for three days, and their physical state, including incision, was closely monitored.

Replanted cell counting

For nucleated cell counting, the precipitate from 1 mL of pre- or post-SECCS-processed bone marrow after centrifugation was mixed with red blood cell lysate (TBD, China) to remove red blood cells, and the number of nucleated cells was counted by a counting machine (Countess II, Thermo Fisher, USA).

To count the number of MSCs, 1 mL of pre- or post-SECCS-processed bone marrow was diluted in the basic

© Annals of Translational Medicine. All rights reserved.

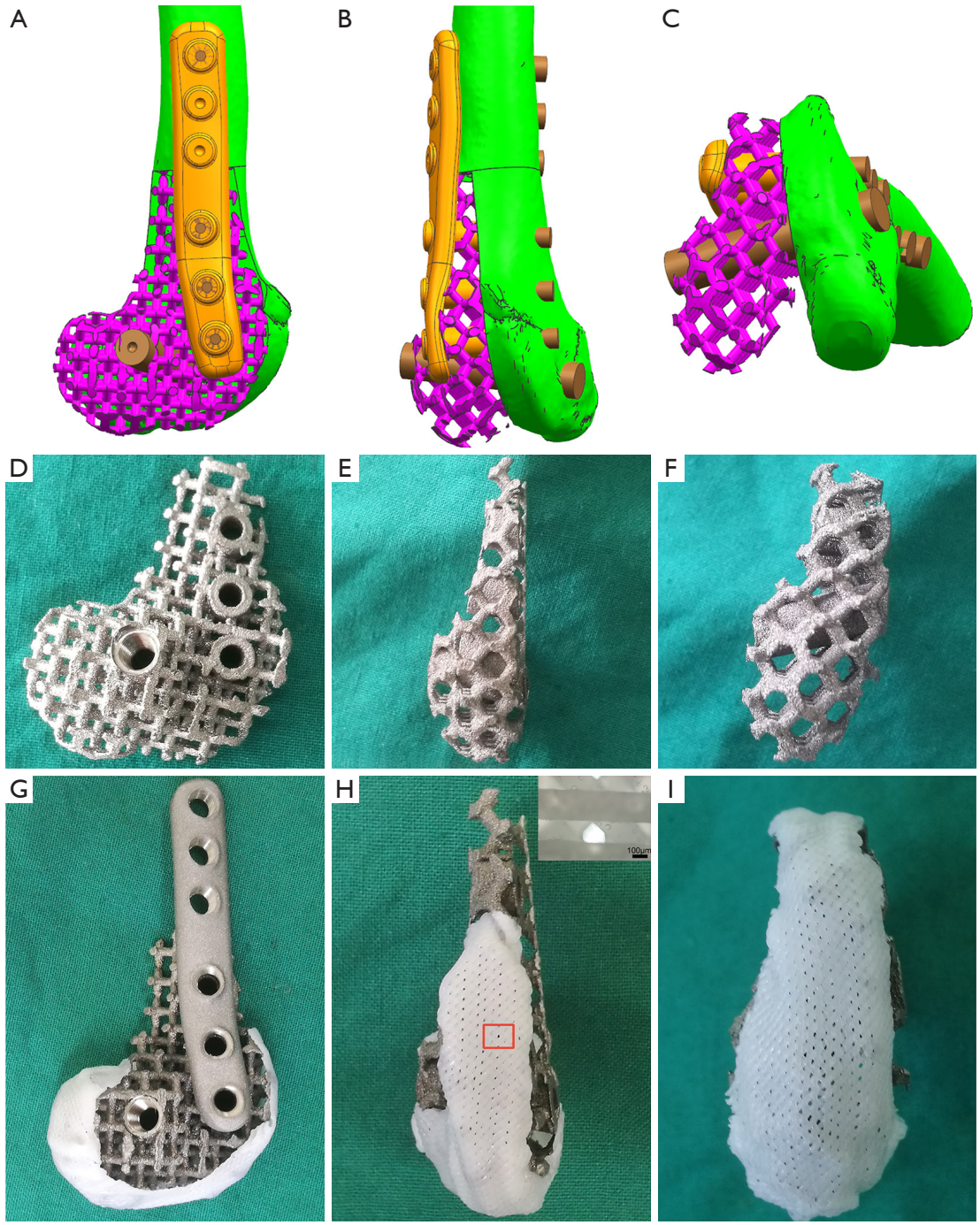

Figure 3 Design and fabrication of the frame matched with the goat's lateral half of the distal femur. (A,B,C) The designed frame with the inner fixation system in the lateral (A), anteroposterior (B), and axial views (C). (D,E,F) The fabricated Ti6Al4V frame in the lateral (D), anteroposterior (E), and axial views (F). (G,H,I) A PCL membrane was attached to the distal surface of the fabricated frame. PCL, poly (ε-caprolactone).

© Annals of Translational Medicine. All rights reserved.

medium and seeded into six-well plates at a density of 0.1 mL/well. After 2 days of culturing, pro-osteogenic medium (α-MEM supplemented with 10% fetal bovine serum, 0.1 mM dexamethasone, 50 mM ascorbic acid, and 10 mM β-glycerophosphate sodium) was added and changed every 2 days at 37 ℃ with 5% CO_2 for osteogenesis of the MSCs. Two weeks later, alkaline phosphatase staining was performed to count the number of CFU/ALP+ as the number of MSCs. In detail, after 20-minute fixation by 4% paraformaldehyde, the cultures were added with ALP stain (Shanghai Hongqiao, China) at 37 ℃ for 1 hour.

The replanted cell number was calculated according to the following formula:

$$N = N_{pre} \times V_{pre} - N_{post} \times V_{post} \quad [1]$$

where N_{pre} and N_{post} represent the number of cells (including NCs and MSCs) per mL of bone marrow pre- and post-SECCS, respectively. V_{pre} and V_{post} stand for the total volume of bone marrow pre- and post-SECCS, respectively.

Evaluations of the bone defect repair

All bone defects were detected by X-ray 1, 3, and 6 months after surgery and CT scans 6 and 9 months after surgery. At 9 months after surgery, all animals were sacrificed, and the surgical part of the distal femur was completely removed. Those samples were fixed with paraformaldehyde at room temperature. The samples were then embedded in polymethyl methacrylate and cut into 100-μm thick slices with a diamond band saw (EXAKT300CP, Norderstedt, Germany) followed by polishing down to 50 μm with a plate grinder (EXAKT310, Norderstedt, Germany) for Van Gieson's picro-fuchsin staining. Briefly, the slides were sequentially treated with 0.1% formic acid for 3 minutes and 20% methanol for 2 hours before being stained with Stevenel's blue at 60 ℃ and Van Gieson's picro-fuchsin at room temperature. The ratios of the new bone area in the frame to the whole slice area between different groups according to the staining using Image-Pro Plus 6.0 were compared.

Statistical analysis

All data were analyzed using SPSS 24.0 software (IBM, USA) and presented as the mean ± standard deviation. The paired *t*-test was used to compare paired data. Differences between multiple data groups were compared by one-way analysis of variance and further by the least significant difference *t*-test, and the Kruskal-Wallis test was used when equal variance was not assumed. P<0.05 was considered to be indicative of statistical significance.

Results

Optimization of printing parameters and the preparation of the repair frames

The cylindrical testing frame's design parameters with regular hexagonal basic structural units were optimized, and then the test frames were made with Ti6Al4V. Three columnar frames with different combinations of width (w) and the inscribed circle diameter (d) of the regular hexagonal unit were prepared: w=1.7 mm, d=4.0 mm; w=1.9 mm, d=4.4 mm and w=2.0 mm, d=5.0 mm. The frame with parameters of w=1.9 mm, d=4.4 mm did not collapse when the load reached 10,000 N, whereas the other two were destroyed before the load reached 10,000 N (*Figure 2B*). Specifically, the maximum load was 9,553.7±51.9 N for the frame with w=1.7 mm, d=4.0 mm; 8,693.6±146.9 N for the frame with w=2.0 mm d=5.0 mm and >10,000 N for the frame with w=1.9 mm, d=4.4 mm; the maximum load was significantly higher for the frame with the latter combination than those for the frames with the other two-parameter combinations (P<0.05) (*Figure 2C*).

A Ti6Al4V frame and internal fixation system with parameters of w=1.9 mm and d=4.4 mm that matched the defect of the 5.3 cm-long lateral half of the distal femur of the goat (*Figure 3A,B,C*) was prepared (*Figure 3D,E,F*). The distal end of the frame was covered with a 2 mm-thick PCL membrane having an average pore size of 132±15.6 μm (*Figure 3G,H,I*).

Biological evaluation of the MSCs/β-TCP prepared by SECCS and the counting of replanted cells

The working SECCS is shown in *Figure 4A*, and SECCS processed the porous β-TCP particles (*Figure 4B*) to prepare the MSCs/β-TCP composites (*Figure 4C*). After the MSCs/β-TCP test samples were cultured *in vitro* for 2 weeks, the cells were observed to adhere to the inner wall of the β-TCP and to have fully spread (*Figure 4D,E*).

After treatment with SECCS, the number of CFU/ALP+ in the goat bone marrow decreased significantly (t=3.078; P=0.037) from 848.3±649.2 per mL to 244.0±212.6 per mL (*Figure 5A,B,C*). There was no significant difference in the decrease of bone marrow nucleated cells (t=1.977, P=0.119)

© Annals of Translational Medicine. All rights reserved.

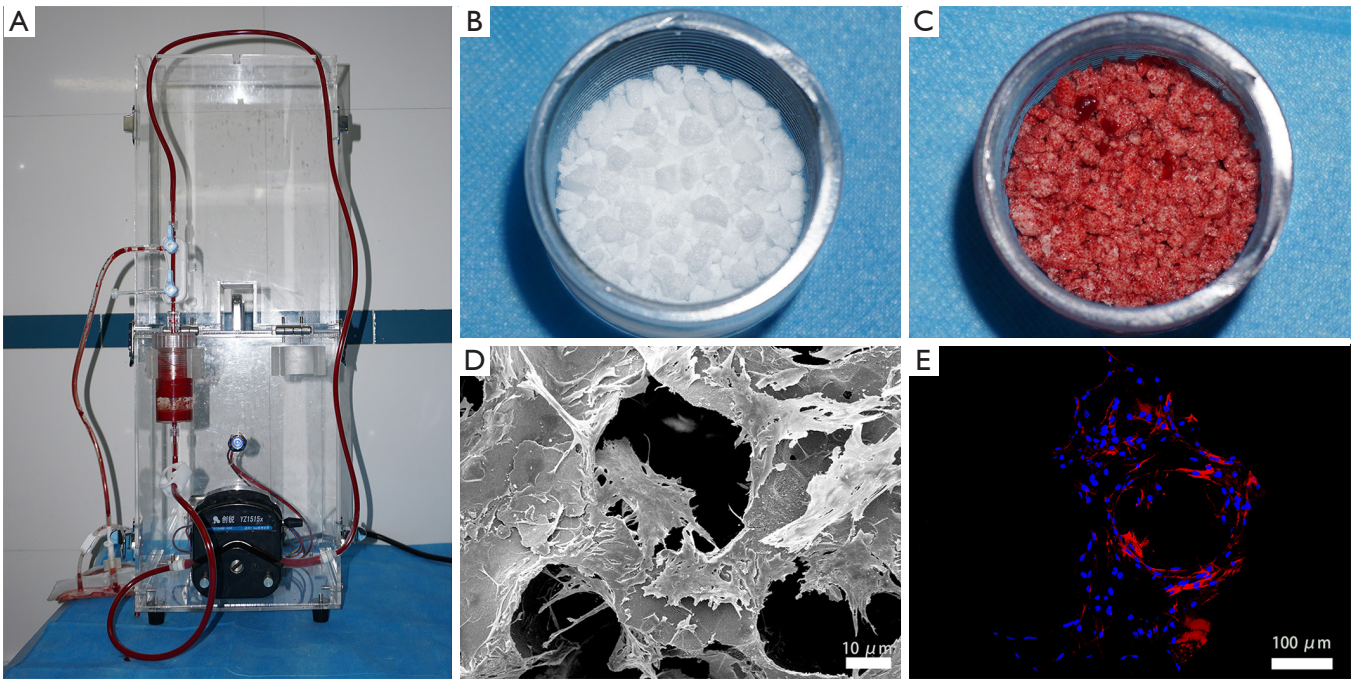

Figure 4 Preparation and characterization of the MSCs/β-TCP. (A) The proprietary Screen–Enrich–Combine(-biomaterials) Circulating System (SECCS) was used to prepare MSCs/β-TCP. (B,C) Porous β-TCP (B) was transformed into MSCs/β-TCP (C) by SECCS. (D,E) Scanning electron microscopy and laser scanning confocal microscopy views show that the cells adhered to and widely spread on to the MSCs/β-TCP particle testing samples' inner wall after 14-day culture. MSC, mesenchymal stem cell; β-TCP, beta tricalcium phosphate.

from 11.9±4.1×10^6 to 11.3±4.5×10^6 per mL (*Figure 5D*). In this study, the average number of replanted MSCs for each goat in the MSCs/β-TCP–filled group was approximately 31,321.7±22,554.7.

Repair of the bone defect in the lateral half of the goat's distal femur

The previously made 5.3 cm-long bone defect in the goat's lateral half of the distal femur and the matching Ti6Al4V frame filled with MSCs/β-TCP particles are shown in *Figure 6*. X-ray radiography showed that particles scattered on the edge of the frame were still seen in the pure β-TCP–filled group but not in the MSCs/β-TCP–filled group at 3 months after the operation. Also, the presence of bone hyperplasia at the proximal fracture site could be observed at 3 months after surgery in the MSCs/β-TCP–filled group, whereas a similar presence could be seen only at 6 months after surgery in the β-TCP–filled group. The X-ray radiography also confirmed a perfect match between the frame and defect (*Figure 7A*). CT could see tissue growth within the blank group frame, pure β-TCP–filled group, and MSCs/β-TCP–filled group at 6 and 9 months after surgery (*Figure 7B*).

Histological analysis was performed to evaluate the new bone growth inside the frame and the osseointegration between the frame and the offside bone. At the junction of the frame and the contralateral bone, good osseointegration was seen in each group's distal section, but osseointegration in the proximal and middle sections was poor. In the blank group, fibrous tissue predominated inside the frame, and only a small amount of new bone was formed. In the β-TCP–filled group, the β-TCP particles were almost completely degraded and substituted mainly by fibrous tissue at each section with a small amount of new bone. In the MSCs/β-TCP–filled group, the material was completely degraded, and new bone formation with normal trabecular structure was seen in each section. Further, a regenerated Haversian system was also observed (*Figure 8A*). Quantitative analysis showed that the relative area of new bone was significantly higher in the MSCs/β-TCP–filled group than in the β-TCP implantation group or the blank group at the proximal section (10.8%±6.0% *vs.* 3.7%±1.7% *vs.* 1.4%±0.9%, respectively; F=10.953, P<0.01), middle

© Annals of Translational Medicine. All rights reserved.

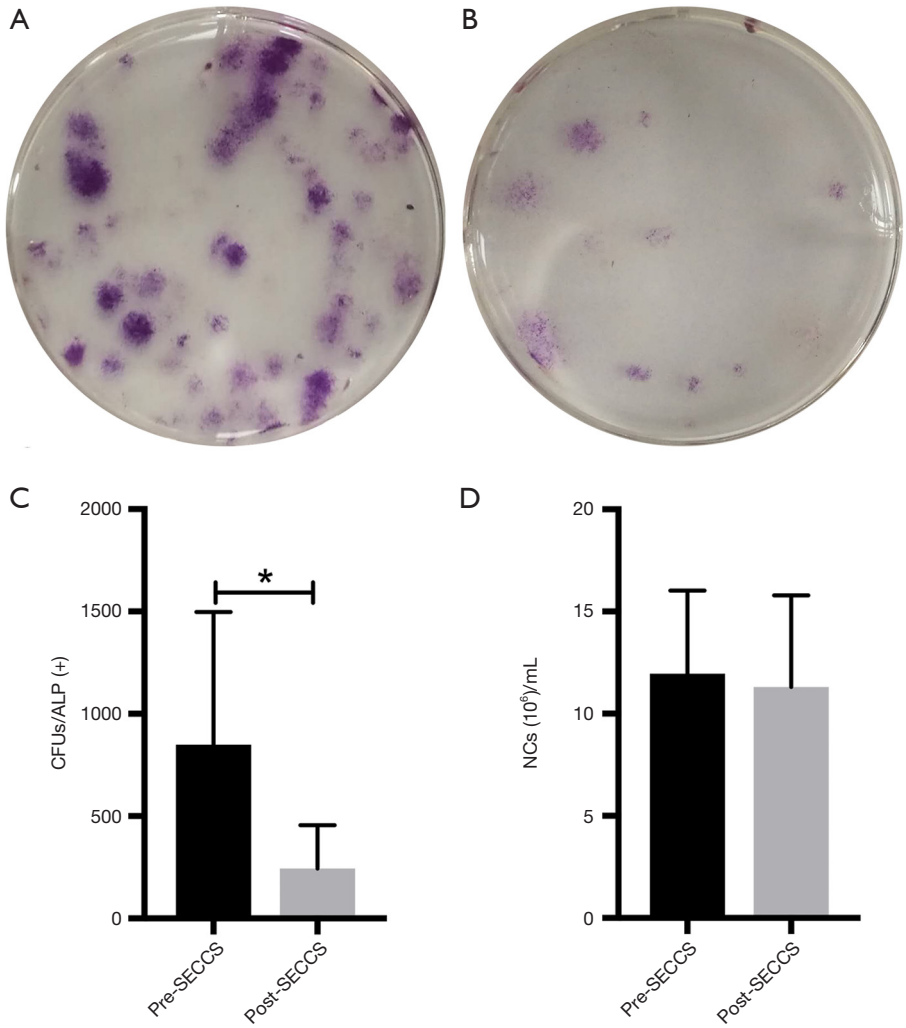

Figure 5 Replanted cell counting. (A,B) The CFU/ALP+ counts from bone marrow before (A), and after (B) Screen–Enrich–Combine(-biomaterials) Circulating System (SECCS) processing was obtained. (C,D) The number of CFU/ALP+ (C) or NCs (D) was reduced remarkably after SECCS processing. CFU/ALP+, alkaline phosphatase-positive colony-forming units; NCs, nucleated cells. ALP staining. *, P<0.05.

section (21.6%±7.8% *vs.* 6.3%±2.6% *vs.* 3.4%±2.1%, respectively; F=24.098, P<0.01), and distal section (41.5%±15.5% *vs.* 15.8±11.0% *vs.* 9.1%±5.3%, respectively; F=13.558, P<0.01) (*Figure 8B,C,D*).

Discussion

Early recovery of weight-bearing function and reconstruction of complex geometries by regenerated autologous bone are the key goals of repairing complex anatomical weight-bearing bone defects. The ideal repair is when shape-matched materials provide sufficient mechanical support and induce new bone to grow quickly and fully during the degradation process. However, currently used degradable materials do not guarantee mechanical support as they degrade. In this study, to achieve bone defect repair with as much autologous bone growth as possible under the condition of early load-bearing, we prepared a macroporous Ti6Al4V frame with a defect-matching shape by 3D printing to provide short-term mechanical support. We filled the frame with osteogenic biomaterial prepared by SECCS to achieve long-term bone repair by regenerated bone. This strategy is a new approach to repair complex anatomical weight-bearing bone defects with both short-

© Annals of Translational Medicine. All rights reserved.

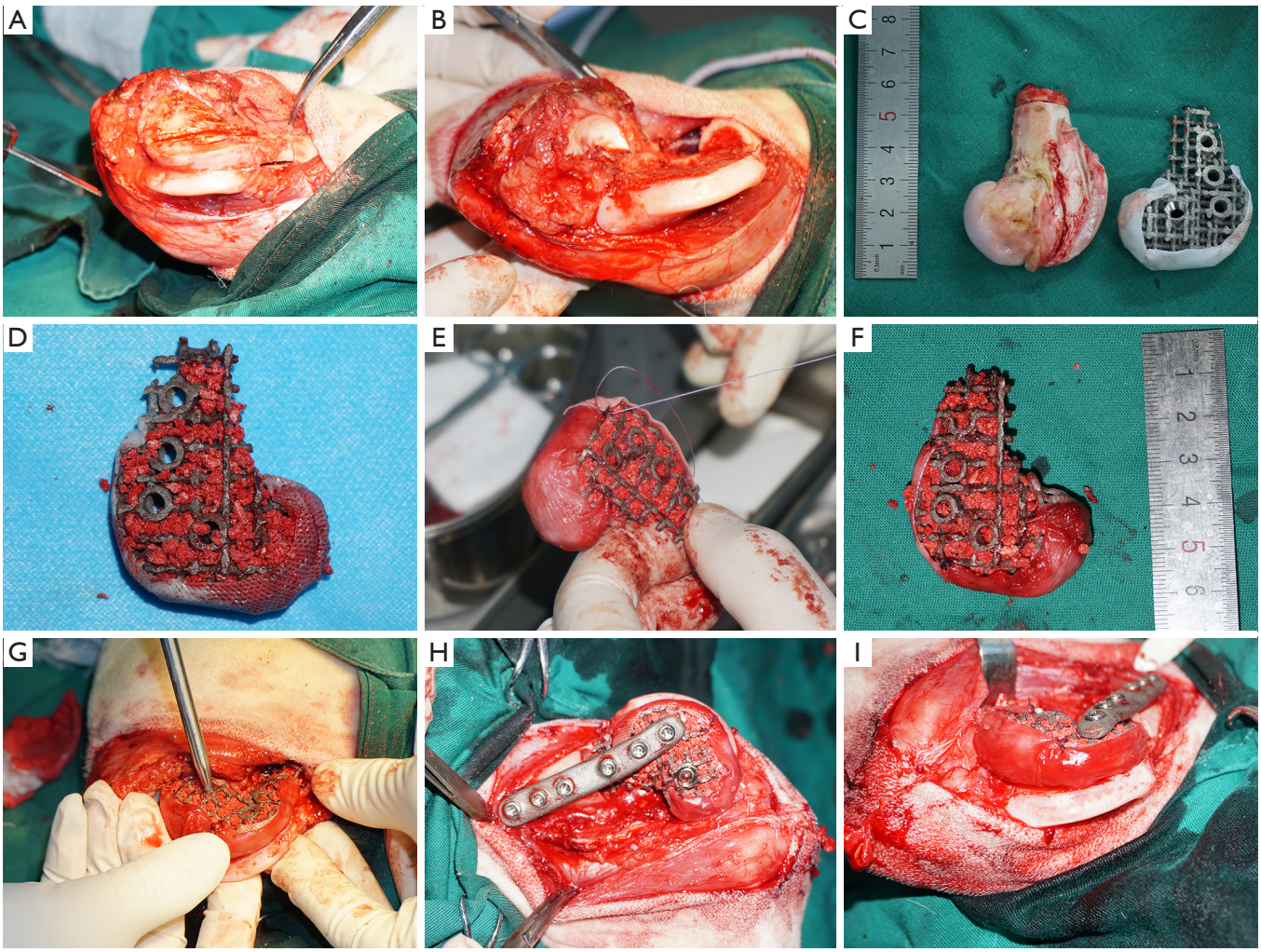

Figure 6 Establishment and repair of a goat bone defect model. (A,B,C) The lateral half of the distal femur was removed to establish the bone defect model. (D,E,F) MSCs/β-TCP particles were filled into the Ti6Al4V frame, and a Bio-Gide membrane was sutured into the PCL layer to round the distal surface. (G,H,I) The prepared frame was fixed in the defect area. MSC, mesenchymal stem cell; β-TCP, beta tricalcium phosphate; PCL, poly (ε-caprolactone).

term and long-term benefits.

Additive manufacturing enables design freedom and manufacturing flexibility, so it has unparalleled advantages in preparing customized implants (12). By its higher-energy density, EBM has become the main method of additive manufacturing for metal implant fabrication in recent years (13). Metal implants prepared by EBM have been used in spinal intervertebral fusion cages and upper cervical vertebral and skull reconstructions (14-16). To enhance implants' long-term stability, most of those prepared by EBM have had a microporous structure to provide the potential for long-term osseous ingrowth. However, the pore size of the microporous structures reported so far have mostly ranged between 100–500 μm, and the volume of bone that can grow is very limited (17). Therefore, the bony holding force produced by this limited new growth bone is restricted. This study replaced the widely used microporous structure with a large-aperture frame structure to leave more space for bone growth.

To select the appropriate printing parameters to ensure the mechanical strength of the frame, we evaluated the mechanical properties of the cylindrical frame with three sets of parameters according to the mechanical test standard (18). Inspired by a honeycomb, in which each

© Annals of Translational Medicine. All rights reserved.

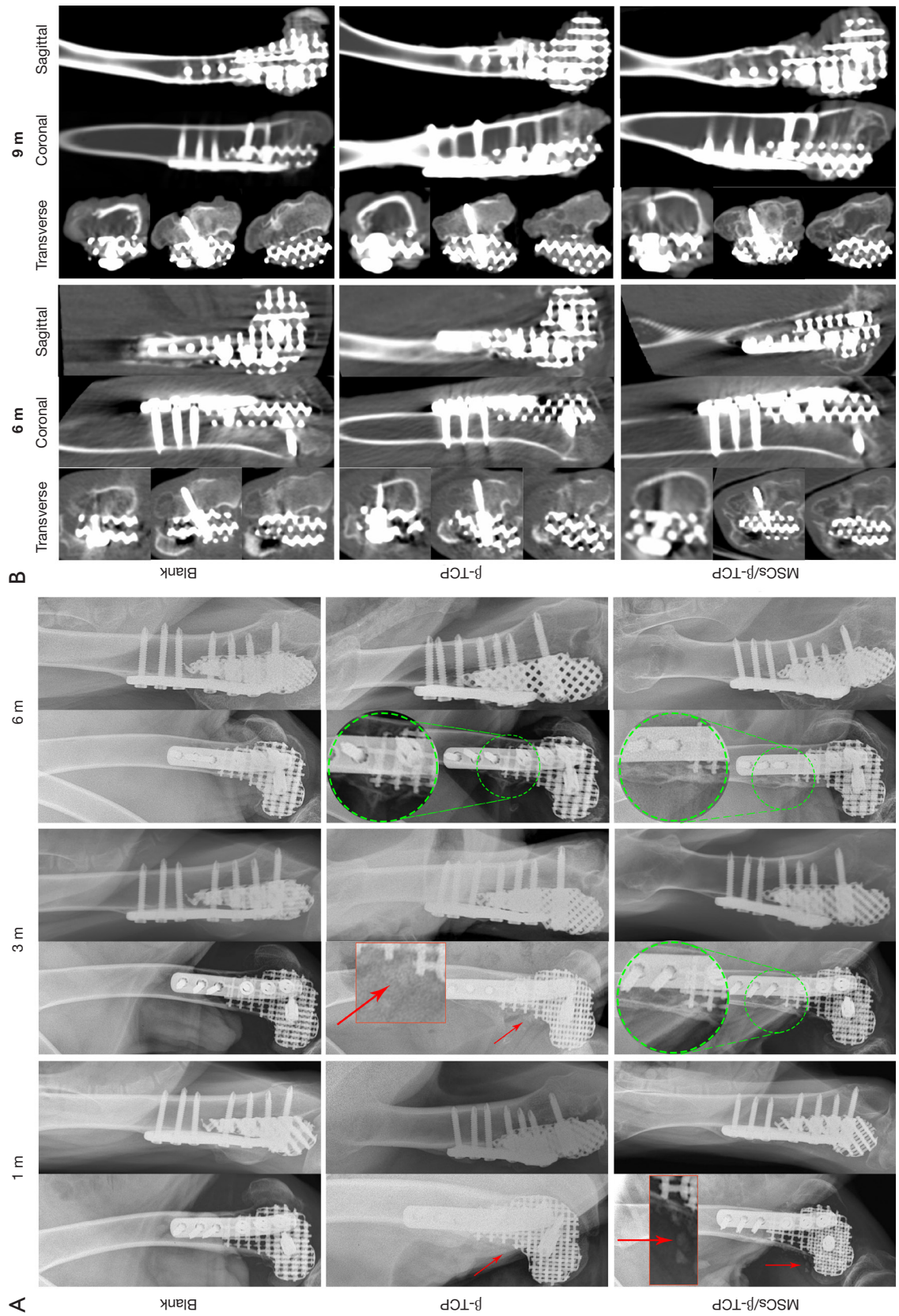

Figure 7 Evaluation of the bone defect repair by imaging examinations. (A) X-ray radiography showed that the frames in each group matched the defect shape perfectly. The presence of particles around the frames (red arrow) is observed in the β-TCP group at 1 and 3 months after surgery and in the MSCs/β-TCP group only 1 month after surgery. The bone hyperplasia presence between bone and frame (green circle) can be seen 3 months after surgery in the MSCs/β-TCP group, but not till 6 months after surgery in the β-TCP group. (B) CT image showing tissue growth in each group's inner frames at 6 and 9 months after surgery. MSC, mesenchymal stem cell; β-TCP, beta tricalcium phosphate.

© Annals of Translational Medicine. All rights reserved.

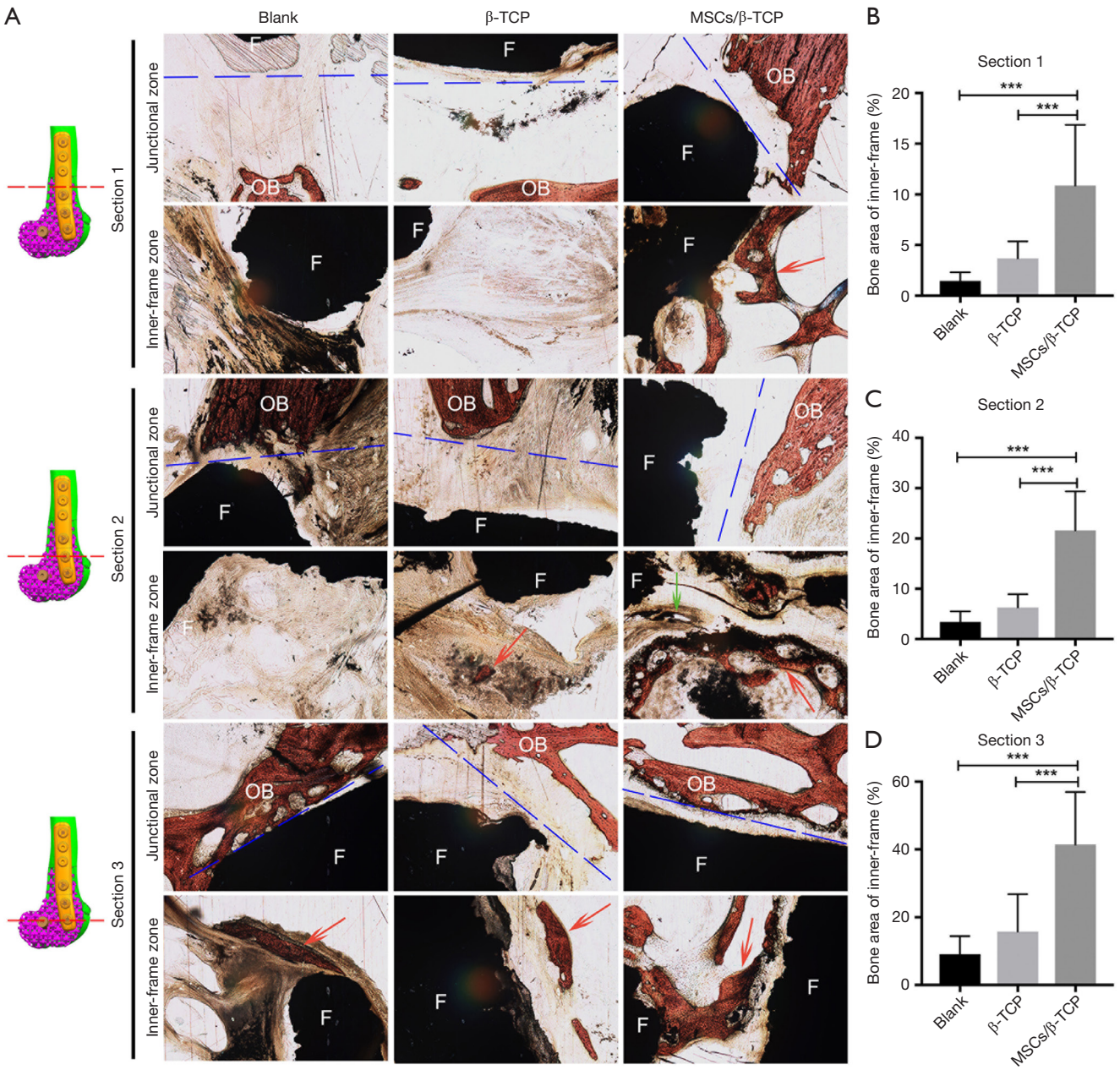

Figure 8 Histological evaluation of the bone defect repair by Van Gieson's picro-fuchsin staining. (A) In the proximal section (section 1), obvious trabecular bone is seen in the inner frame zone in the MSCs/β-TCP group despite suboptimal bone integration at the junctional site between the contralateral side and frame in each group. In the middle section (section 2), there is still no obvious sign of bone growth from the contralateral side at the junctional site in each group; however, new bone with the Haver's system has abundantly filled the inner frame in the MSCs/β-TCP group, whereas there is limited new bone growth in the β-TCP group and almost no bone growth in the blank group. In the distal section (section 3), optional bone integration at the junctional site is seen in each group, but only in the MSCs/β-TCP group did new trabecular bone form. (B,C,D) Quantitative analysis of the bone area within the frames can be seen in each section. (The blue dotted line represents the dividing line between the frame and offside bone; 'F' and 'OB' stand for the frame and offside bone, respectively, and the 'Red arrow' and 'Green arrow' point to the new bone and the Haver's system, respectively). MSC, mesenchymal stem cell; β-TCP, beta tricalcium phosphate. ***, P<0.001. Magnification: × 5.

© Annals of Translational Medicine. All rights reserved.

comb is connected to other combs on all six sides and achieves good space utilization with less material, we used a regular hexagonal basic printing unit. The width of the side and the diameter of the hexagonal units' inscribed circle are the two key factors that affect the overall mechanical properties of the frame. Theoretically, a larger inscribed circle diameter provides more space for a bone filling but reduces the mechanical strength, whereas the opposite relationship is observed for the side's width. In this study, the frame with the combination of w=1.9 mm and d=4.4 mm for the hexagonal units had a better mechanical performance, indicating that the mechanical increment caused by the increase in the side width from 1.7 to 1.9 mm exceeded the mechanical decrement caused by the increase in the inscribed circle diameter from 4.0 to 4.4 mm.

Additionally, the mechanical increase by increasing the side width from 1.9 mm to 2.0 mm did not exceed the mechanical decrease by increasing the inscribed circle diameter from 4.4 to 5.0 mm. Consequently, we used the optimal width and diameter parameters to prepare the Ti6Al4V frame, which matched the goat's distal femur's lateral half. The corresponding internal fixation system was designed and fabricated at the same time. Since the defect model involved the articular surface, a PCL film was used to cover the frame's distal end to improve smoothness and reduce rigidity to minimize potential joint damage. Also, a Bio-Gide collagen membrane was sutured into the PCL film's surface to protect the joints further.

The osteogenic ability of bone fillers is the key to bone defect repair. Since autologous bone grafting, which currently is the gold standard for bone grafting treatment, has some disadvantages, such as limited supply and bone-collecting–related complications, finding bone substitutes with similar osteogenic ability has always been an important goal in orthopedic research (19). Bone marrow MSCs are indispensable for bone repair (20,21). Many studies have confirmed that the use of MSCs with bone substitutes can effectively promote the bone repair effect (22-24). The SECCS we developed previously can rapidly incorporate screening, enrichment of autologous bone marrow MSCs, and generation of composites with porous bone substitutes intraoperatively. These composites have shown superior osteogenic effects in animal models and clinical patients (10,25). In this study, the number of MSCs in the bone marrow was significantly decreased after treatment with SECCS, indicating that MSCs successfully adhered to the porous β-TCP (10). From the testing particles, the adhered MSCs were widely distributed on the inner wall of the β-TCP and fully spread. The number of bone marrow MSCs replanted is an important factor in determining the effect of bone repair (26,27). In this study, each goat was replanted with approximately 31,321.7±22,554.7 MSCs on average in the MSCs/β-TCP–filled group. In the reported studies on bone tissue engineering, most of the implanted MSCs were obtained through *in vitro* culture, and the number of transplanted MSCs often reached millions, which was much higher than that achieved in this study (22,23). In this regard, we believe that SECCS has the following advantages over *in vitro* culture technology that outweighs its relatively lower number of replants. Although the number of MSCs expanded *in vitro* was huge, they originated from a small number of primary cells. In terms of replanted primary MSCs, SECCS showed an overwhelming advantage. Since MSCs will inevitably undergo replicative senescence during *in vitro* culture, the proliferation and differentiation ability of MSCs will be reduced to a certain extent after expansion, whereas the MSCs replanted by SECCS retain their original ability (28,29). Second, the bone marrow MSCs that expanded *in vitro* experienced sudden changes in the living environment after implantation into the body, potentially inhibiting cell viability. However, the cells replanted by SECCS were not cultured *in vitro*, circumventing this inhibitory factor.

The goat distal femur's lateral half had both partial weight-bearing function and complex geometry and was easy to expose and observe. Therefore, it was used as a bone defect model in this study. Intraoperative photos and postoperative X-rays showed that the frame prepared by 3D printing completely matched the defect shape, and the shape was still well maintained 9 months after surgery. Postoperative X-ray radiograms showed that the scattered particles around the frame in the MSCs/β-TCP–the filled group had degraded and disappeared by 3 months after surgery, whereas those in the β-TCP–filled group were still visible at 3 months after surgery, suggesting that the former had a relatively faster degradation rate than that of the latter, which is consistent with the results found in our previous study (30). Also, the bony bridging presence at the proximal fracture site was seen earlier in the MSCs/β-TCP–filled group than in the β-TCP–filled group, which may have been related to the recruitment of autologous MSCs by implanted MSCs to promote local bone ingrowth (31,32). From the CT results, even though we rounded the frame's distal end, there was still joint damage, such as patella displacement and joint wear. This finding may be

© Annals of Translational Medicine. All rights reserved.

because the end of the frame damaged the outer protective complex during the wear process. Therefore, it may be more appropriate for defects with joint retention to adopt a frame with a non-porous and polished surface. In terms of defect repair, the CT results showed that tissue ingrowth was present even in the frames without material filling, suggesting that a microporous structure may not be necessary for tissue ingrowth. Due to the interference by metal artifacts, we could not evaluate the tissue composition based on the tissue's grey value within the frame.

To observe the osteogenesis effect inside the frame, we performed segmented slices of the repaired frame. A better bone construction effect within the frame could be seen at each section in the MSCs/β-TCP–filled group, with the new trabecular bone tightly integrated with the frame wall and the Harval system under reconstruction, which suggests that the new bone has good plasticity. Generally, the new bone area at the distal section accounts for a relatively large proportion of the area. This characteristic may be due to the larger contact area between the distal part and the contralateral normal bone, which results in a more complete local osteogenesis environment. Studies have shown that the degradation cycle of porous β-TCP is between 6 to 18 months. In this study, the porous β-TCP with a diameter of 1–3 mm implanted in the defect region was almost degraded by 9 months after surgery, consistent with previous reports.

Interestingly, in the pure β-TCP–filled group, a small new bone island appeared at the center of the filling area, suggesting that the new bone formation mode mediated by porous materials did not completely depend on the gradual replacement from the surrounding normal bone to the material pores. The ossification process may also occur independently inside the porous material, possibly through the penetrated bone marrow. Although the CT results indicated tissue ingrowth in the three groups, the amount of new bone in the blank group and β-TCP–the filled group was very limited and mainly manifested as fibrous scar tissue. Accordingly, the filler's osteogenic capacity significantly affected the long-term osteogenic effect, and the MSCs/β-TCP prepared by SECCS exhibited better osteogenic performance in this defect model.

In this study, in response to the clinical problem of complex anatomical bone defects in weight-bearing areas, we proposed and assessed an approach to achieve bone repair by providing a larger volume of final autologous bone; this approach involved preparing a large-aperture weight-bearing frame by 3D printing and placement of biomaterials modified by SECCS in the frame to achieve long-term bone filling. This approach may provide a new treatment option for the clinical repair of such bone defects. However, the limitations of this study should not be ignored. Foremost was the outer protective complex design, which was degradable and eventually allowed the protruded frame to end to damage the joint. Although we evaluated the effect of MSCs replanted through SECCS on bone repair, the working mechanism of this effect was not elucidated.

Conclusions

Filling a 3D-printed Ti6Al4V large-aperture frame with osteogenic materials provided a greater extent of biological reconstruction for bone defects with a complex anatomical shape in the weight-bearing part under the condition of early weight-bearing. MSCs/β-TCP prepared by SECCS can be used as a filling material for this type of bone defect to obtain a good bone repair effect.

Acknowledgments

The authors sincerely thank Lu Shen for instructions in software usage and also acknowledge Wendong Xue for his help with the mechanical test.

Funding: This work was supported by the Clinical Research Program of the Ninth People's Hospital, Shanghai Jiao Tong University School of Medicine [JYLJ015] and the Clinical Research Plan of SHDC [16CR3099B], the Class IV Peak Subject Program of Shanghai Jiao Tong University School of Medicine (no. GXQ03), and the National Key Research and Development Program of China (2016YFC1102104, 2017YFC1103900).

Footnote

Reporting Checklist: The authors have completed the ARRIVE reporting checklist. Available at http://dx.doi.org/10.21037/atm-20-6689

Data Sharing Statement: Available at http://dx.doi.org/10.21037/atm-20-6689

Peer Review File: Available at http://dx.doi.org/10.21037/atm-20-6689

Conflicts of Interest: All authors have completed the ICMJE

© Annals of Translational Medicine. All rights reserved.

uniform disclosure form (available at http://dx.doi.org/10.21037/atm-20-6689). The authors have no conflicts of interest to declare.

Ethical Statement: The authors are accountable for all aspects of the work in ensuring that questions related to the accuracy or integrity of any part of the work are appropriately investigated and resolved. All experimental procedures in this study were approved and performed under a project license {HKDL [2017] 405} granted by the Animal Ethics Committee of Shanghai Ninth People's Hospital, in compliance with the Shanghai Ninth People's Hospital affiliated with the Shanghai Jiao Tong University School of Medicine guidelines for the care and use of animals.

Open Access Statement: This is an Open Access article distributed in accordance with the Creative Commons Attribution-NonCommercial-NoDerivs 4.0 International License (CC BY-NC-ND 4.0), which permits the non-commercial replication and distribution of the article with the strict proviso that no changes or edits are made and the original work is properly cited (including links to both the formal publication through the relevant DOI and the license). See: https://creativecommons.org/licenses/by-nc-nd/4.0/.

References

1. Anract P, Biau D, Babinet A, et al. Pelvic reconstructions after bone tumor resection. Bull Cancer 2014;101:184-94.
2. Migaud H, Common H, Girard J, et al. Acetabular reconstruction using porous metallic material in complex revision total hip arthroplasty: A systematic review. Orthop Traumatol Surg Res 2019;105:S53-61.
3. Struckmann V, Schmidmaier G, Ferbert T, et al. Reconstruction of Extended Bone Defects Using Massive Allografts Combined with Surgical Angiogenesis: A Case Report. JBJS Case Connect 2017;7:e10.
4. Du YQ, Liu YP, Sun JY, et al. Reconstruction of Paprosky type IIIB acetabular bone defects using a cup-on-cup technique: A surgical technique and case series. World J Clin Cases 2020;8:1223-31.
5. Zhang Z, Zhao J, Huang X, et al. Short-term effectiveness of acetabular reconstruction with three-dimensional printed trabecular metal pads in hip revision. Zhongguo Xiu Fu Chong Jian Wai Ke Za Zhi 2019;33:1516-20.
6. Sporer SM, O'Rourke M, Chong P, et al. The use of structural distal femoral allografts for acetabular reconstruction. Average ten-year follow-up. J Bone Joint Surg Am 2005;87:760-5.
7. Costa Mendes L, Sauvigne T, Guiol J. Morbidity of autologous bone harvesting in implantology: Literature review from 1990 to 2015. Rev Stomatol Chir Maxillofac Chir Orale 2016;117:388-402.
8. Seiler JG 3rd, Johnson J. Iliac crest autogenous bone grafting: donor site complications. J South Orthop Assoc 2000;9:91-7.
9. Busch A, Wegner A, Haversath M, et al. Bone Substitutes in Orthopaedic Surgery: Current Status and Future Perspectives. Z Orthop Unfall 2020. [Epub ahead of print]. doi: 10.1055/a-1073-8473.
10. Chu W, Gan Y, Zhuang Y, et al. Mesenchymal stem cells and porous beta-tricalcium phosphate composites prepared through stem cell screen-enrich-combine(-biomaterials) circulating system for the repair of critical size bone defects in goat tibia. Stem Cell Res Ther 2018;9:157.
11. Zhuang Y, Gan Y, Shi D, et al. A novel cytotherapy device for rapid screening, enriching and combining mesenchymal stem cells into a biomaterial for promoting bone regeneration. Sci Rep 2017;7:15463.
12. Martin JH, Yahata BD, Hundley JM, et al. 3D printing of high-strength aluminium alloys. Nature 2017;549:365-9.
13. Parthasarathy J, Starly B, Raman S, et al. Mechanical evaluation of porous titanium (Ti6Al4V) structures with electron beam melting (EBM). J Mech Behav Biomed Mater 2010;3:249-59.
14. Wei F, Li Z, Liu Z, et al. Upper cervical spine reconstruction using customized 3D-printed vertebral body in 9 patients with primary tumors involving C2. Ann Transl Med 2020;8:332.
15. Epasto G, Distefano F, Mineo R, et al. Subject-specific finite element analysis of a lumbar cage produced by electron beam melting. Med Biol Eng Comput 2019;57:2771-81.
16. Francaviglia N, Maugeri R, Odierna Contino A, et al. Skull Bone Defects Reconstruction with Custom-Made Titanium Graft shaped with Electron Beam Melting Technology: Preliminary Experience in a Series of Ten Patients. Acta Neurochir Suppl 2017;124:137-41.
17. Zhang L, Yang G, Johnson BN, et al. Three-dimensional (3D) printed scaffold and material selection for bone repair. Acta Biomater 2019;84:16-33.
18. Xie XH, Wang XL, Zhang G, et al. Biofabrication of a PLGA-TCP-based porous bioactive bone substitute with sustained release of icaritin. J Tissue Eng Regen Med 2015;9:961-72.

© Annals of Translational Medicine. All rights reserved.

19. Ebraheim NA, Elgafy H, Xu R. Bone-graft harvesting from iliac and fibular donor sites: techniques and complications. J Am Acad Orthop Surg 2001;9:210-8.
20. Lin W, Xu L, Zwingenberger S, et al. Mesenchymal stem cells homing to improve bone healing. J Orthop Translat 2017;9:19-27.
21. Hernigou P, Poignard A, Beaujean F, et al. Percutaneous autologous bone-marrow grafting for nonunions. Influence of the number and concentration of progenitor cells. J Bone Joint Surg Am 2005;87:1430-7.
22. Liu G, Zhao L, Zhang W, et al. Repair of goat tibial defects with bone marrow stromal cells and beta-tricalcium phosphate. J Mater Sci Mater Med 2008;19:2367-76.
23. Viateau V, Guillemin G, Bousson V, et al. Long-bone critical-size defects treated with tissue-engineered grafts: a study on sheep. J Orthop Res 2007;25:741-9.
24. Gan Y, Dai K, Zhang P, et al. The clinical use of enriched bone marrow stem cells combined with porous beta-tricalcium phosphate in posterior spinal fusion. Biomaterials 2008;29:3973-82.
25. Wang X, Chu W, Zhuang Y, et al. Bone Mesenchymal Stem Cell-Enriched beta-Tricalcium Phosphate Scaffold Processed by the Screen-Enrich-Combine Circulating System Promotes Regeneration of Diaphyseal Bone Non-Union. Cell Transplant 2019;28:212-23.
26. Wu H, Kang N, Wang Q, et al. The Dose-Effect Relationship Between the Seeding Quantity of Human Marrow Mesenchymal Stem Cells and In Vivo Tissue-Engineered Bone Yield. Cell Transplant 2015;24:1957-68.
27. Petite H, Viateau V, Bensaid W, et al. Tissue-engineered bone regeneration. Nat Biotechnol 2000;18:959-63.
28. Sethe S, Scutt A, Stolzing A. Aging of mesenchymal stem cells. Ageing Res Rev 2006;5:91-116.
29. Ksiazek K. A comprehensive review on mesenchymal stem cell growth and senescence. Rejuvenation Res 2009;12:105-16.
30. Chu W, Wang X, Gan Y, et al. Screen-enrich-combine circulating system to prepare MSC/β-TCP for bone repair in fractures with depressed tibial plateau. Regen Med 2019;14:555-69.
31. Baraniak PR, McDevitt TC. Stem cell paracrine actions and tissue regeneration. Regenerative medicine 2010;5:121-43.
32. Seebach E, Freischmidt H, Holschbach J, et al. Mesenchymal stroma cells trigger early attraction of M1 macrophages and endothelial cells into fibrin hydrogels, stimulating long bone healing without long-term engraftment. Acta biomaterialia 2014;10:4730-41.

Cite this article as: Chu W, Liu Z, Gan Y, Chang Y, Jiao X, Jiang W, Dai K. Use of a novel Screen–Enrich–Combine(-biomaterials) Circulating System to fill a 3D-printed open Ti6Al4V frame with mesenchymal stem cells/β-tricalcium phosphate to repair complex anatomical bone defects in load-bearing areas. Ann Transl Med 2021;9(6):454. doi: 10.21037/atm-20-6689

© Annals of Translational Medicine. All rights reserved.